LETTER

doi:10.1038/nature13731

Global covariation of carbon turnover times with climate in terrestrial ecosystems

Nuno Carvalhais[1,2], Matthias Forkel[1], Myroslava Khomik[1,3], Jessica Bellarby[4,5], Martin Jung[1], Mirco Migliavacca[1,6], Mingquan Mu[7], Sassan Saatchi[8], Maurizio Santoro[9], Martin Thurner[1], Ulrich Weber[1], Bernhard Ahrens[1], Christian Beer[1,10], Alessandro Cescatti[11], James T. Randerson[7] & Markus Reichstein[1]

The response of the terrestrial carbon cycle to climate change is among the largest uncertainties affecting future climate change projections[1,2]. The feedback between the terrestrial carbon cycle and climate is partly determined by changes in the turnover time of carbon in land ecosystems, which in turn is an ecosystem property that emerges from the interplay between climate, soil and vegetation type[3–6]. Here we present a global, spatially explicit and observation-based assessment of whole-ecosystem carbon turnover times that combines new estimates of vegetation and soil organic carbon stocks and fluxes. We find that the overall mean global carbon turnover time is 23^{+7}_{-4} years (95 per cent confidence interval). On average, carbon resides in the vegetation and soil near the Equator for a shorter time than at latitudes north of 75° north (mean turnover times of 15 and 255 years, respectively). We identify a clear dependence of the turnover time on temperature, as expected from our present understanding of temperature controls on ecosystem dynamics. Surprisingly, our analysis also reveals a similarly strong association between turnover time and precipitation. Moreover, we find that the ecosystem carbon turnover times simulated by state-of-the-art coupled climate/carbon-cycle models vary widely and that numerical simulations, on average, tend to underestimate the global carbon turnover time by 36 per cent. The models show stronger spatial relationships with temperature than do observation-based estimates, but generally do not reproduce the strong relationships with precipitation and predict faster carbon turnover in many semi-arid regions. Our findings suggest that future climate/carbon-cycle feedbacks may depend more strongly on changes in the hydrological cycle than is expected at present and is considered in Earth system models.

The largest global gross exchanges of carbon occur at the interface between the atmosphere and the terrestrial biosphere[7]. Changes in the net exchange of CO_2 between the land and the atmosphere may provide positive or negative feedbacks to increasing atmospheric CO_2 concentrations and, thus, changes in climate[1,8]. The response of the net exchange of CO_2 to climate depends on the response of carbon uptake (gross primary production (GPP)) and on how carbon residence times change simultaneously. It is thus of importance to quantify the time that carbon resides in terrestrial ecosystems and its spatial covariation with climate. Furthermore, global modelling studies show a stronger convergence of GPP estimates in comparison with wider ranges in whole ecosystem carbon stocks[9], reflecting the strong spread in the modelled residence times of carbon.

In steady state, that is, when the exchange of carbon between two reservoirs is balanced, the turnover time (τ, yr) equals the mean residence time[10]. Assuming a balance between assimilation and losses of ecosystem carbon, τ can be calculated from the total reservoir size (C_{total}, $\mathrm{kgC\,m^{-2}}$) and the influx or the outflux ($\mathrm{kgC\,m^{-2}\,yr^{-1}}$) as[10]

$$\tau = C_{\mathrm{total}}/\mathrm{flux} \quad (1)$$

For terrestrial ecosystems, the total reservoir size equals the carbon stocks in vegetation and soils. The influx is the carbon uptake through gross primary production GPP and the outflux includes all carbon losses (terrestrial ecosystem respiration, fire emissions, lateral export and so on). We relax the strict steady-state assumption, calling τ the apparent whole ecosystem turnover time, computed as the ratio of C_{total} to GPP, and interpret the quantity as an emergent diagnostic at the ecosystem level (Methods section on turnover times). We note that the turnover time, or mean residence time, of carbon in ecosystems emerges from the turnover of compartments varying greatly in their individual turnover times[5,11] (for example leaves, wood, different soil organic carbon fractions). Hence, carbon allocation, leaf, root and wood turnover, plant mortality and soil carbon decomposition are key processes that regulate the terrestrial turnover times, and which are controlled by climate variability[12].

Here we combine and enhance recently derived estimates of the carbon stocks in vegetation and soil to obtain global total terrestrial ecosystem carbon stocks and their observation-based uncertainties at 0.5° resolution (Methods section on global carbon estimates). We merge remote-sensing-based carbon stock estimates for tropical and Northern Hemisphere vegetation (Methods section on vegetation carbon) with enhanced soil organic carbon estimates based on the Harmonized World Soil Database (HWSD) and a dedicated circumpolar soil organic carbon map (which better accounts for carbon in permafrost-affected high-latitude soils; Methods section on soil organic carbon). Total soil organic carbon stocks are estimated down to full depth (that is, beyond the 100 cm depths often reported, but see Methods section on soil organic carbon). Total carbon stocks (soils and vegetation) amount to $2{,}807^{+855}_{-555}$ Pg of carbon C (PgC) and are predominantly within tropical forests, which contain almost 25% of the total global stocks, followed by boreal forests (18%) (Methods section on global carbon estimates). Per unit area, the total carbon stocks vary largely between and within biomes (Fig. 1a), where tropical forests and northern high latitudes exhibit the highest stocks. Substantial uncertainties are located in tundra regions (interquartile range over the mean, ~38%) and in tropical savannahs and grasslands (~30%) (Extended Data Fig. 1 and Extended Data Table 1).

Using these total ecosystem stocks and the observation-based GPP estimates in equation (1), we derive a global τ of 23 yr (ranging between 18 yr (percentile 2.5) and 29 yr (percentile 97.5)). We note that this duration is an estimation of the mean residence time of a carbon atom in terrestrial ecosystems from its initial fixation by photosynthesis until its respiratory (including autotrophic respiration) or non-respiratory

[1]Max Planck Institute for Biogeochemistry, Hans Knöll Strasse 10, 07745 Jena, Germany. [2]Departamento de Ciências e Engenharia do Ambiente, DCEA, Faculdade de Ciências e Tecnologia, FCT, Universidade Nova de Lisboa, 2829-516 Caparica, Portugal. [3]School of Geography and Earth Sciences, McMaster University, Hamilton, Ontario L8S 4K1, Canada. [4]Institute of Biological and Environmental Sciences, School of Biological Sciences, University of Aberdeen, Aberdeen AB24 3UU, UK. [5]Lancaster Environment Centre, Lancaster University, Bailrigg, Lancaster LA1 4YQ, UK. [6]Remote Sensing of Environmental Dynamics Lab, DISAT, University of Milano-Bicocca, Piazza della Scienza 1, 20126 Milan, Italy. [7]Department of Earth System Science, University of California Irvine, Irvine, California 92697, USA. [8]Jet Propulsion Laboratory, California Institute of Technology, Pasadena, California 91109, USA. [9]Gamma Remote Sensing, Worbstrasse 225, 3073 Gümligen, Switzerland. [10]Department of Applied Environmental Science and Bolin Centre for Climate Research, Stockholm University, Svante Arrhenius väg 8, 10691 Stockholm, Sweden. [11]European Commission, Joint Research Centre, Institute for Environment and Sustainability, Climate Risk Management Unit, Via E. Fermi, 2749, I-21027 Ispra, Italy.

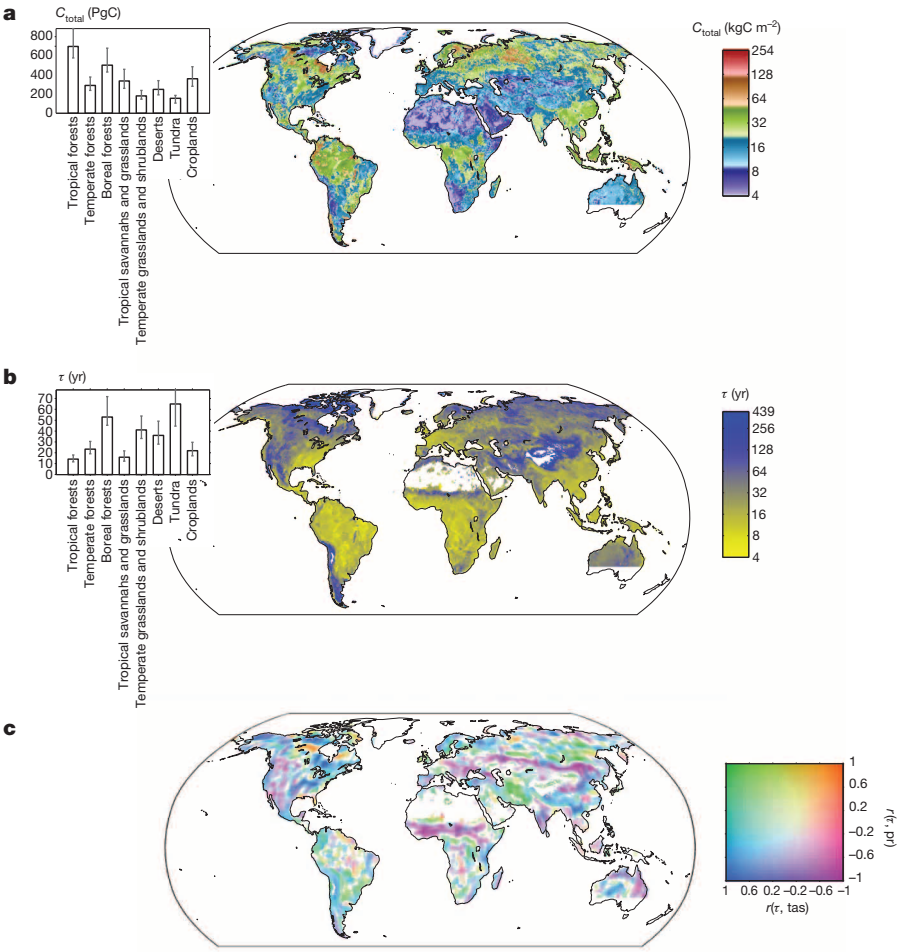

Figure 1 | Global distributions of total ecosystem carbon, turnover times of carbon in terrestrial ecosystems and its spatial covariation with climate variables. Global distribution of estimated total ecosystem carbon (C_{total}) density in each grid cell (kgC m^{-2}), and total ecosystem carbon mass per biome (PgC)) (**a**), median of turnover times of carbon (τ) in terrestrial ecosystems (**b**), and the spatial covariation (r, Pearson correlation coefficient) of τ with climate variables (**c**). The insets in **a** and **b** show the C_{total} and τ estimates per biome according to previous classifications (Extended Data Table 1); the uncertainty bars per biome report the 95% confidence intervals (CI, ranging between percentiles 2.5 and 97.5). The ranges in C_{total} span 4 kgC m^{-2} (approximately the 5th percentile) to 254 kgC m^{-2} (maximum estimate of mean carbon stocks), and the colour code in the τ map is binned between $\tau \leq 4$ yr and 439 yr (the 99th percentile). Spatial correlations (moving window of 5.5° by 5.5°) with temperature (tas) and precipitation (pr) are shown only for confidence levels above 95%. The missing regions in southern Australia and New Zealand are due to missing data in the vegetation carbon data set (Methods section on total vegetation carbon).

loss. A previous collection of global estimates of net primary production, carbon in soils and carbon in vegetation allows an approximate mean estimate of τ of 21 ± 7 yr, assuming 50% of autotrophic respiration costs[13]. Still, the spatial variation of τ observed in our analysis spans almost two orders of magnitude, that is, between ~7 yr (first percentile) and 439 yr (99th percentile) (Fig. 1b and Methods section on mean carbon turnover times).

The longest turnover times are found in cold biomes (tundra, 65^{+13}_{-20} yr; boreal forests, 53^{+20}_{-8} yr), in temperate grassland and shrubland (41^{+13}_{-9} yr) and in desert regions (36^{+14}_{-9} yr), whereas tropical forests and savannah exhibit the shortest turnover times (14^{+4}_{-3} and 16^{+6}_{-4} yr, respectively) (Table 1). Using localized regression analysis (Methods section on correlation analysis), we find that, spatially, τ covaries significantly ($P < 0.05$) with mean annual temperature or with total annual precipitation in 86% of the globe (Fig. 1c and Supplementary Information Section 2). There is, however, a strong variability in the spatial correlations between τ and temperature and τ and precipitation (Fig. 1c and Extended Data Fig. 2). Negative correlations between temperature and τ are widely observed, and can be linked to the expected decomposition responses to temperature[14–16]. However, significant positive correlations emerge in regions of forest/herbaceous cover transitions (or patchiness) and in warm arid environments (Supplementary Information Section 4), where precipitation shows the strongest correlations with τ, indicating that moisture effects may dominate and override temperature effects. No clear dominant patterns are observed in tropical forests, suggesting that climate has a limited effect on the spatial variability of τ there and that nutrient availability[17] or natural and human disturbances[18,19], or both, have greater effects. Globally, we observe a higher frequency of stronger spatial correlations between τ and precipitation (in ~55% of land grid cells) than between τ and temperature (~45%) (Extended Data Figs 3 and 4).

Table 1 | Total ecosystem turnover times of carbon for the globe, per biome

Biome type	τ (yr)		
	Mean	P 2.5	P 97.5
Tropical forests	14.2	11.6	18.2
Temperate forests	23.5	18.9	30.8
Boreal forests	53.3	45.4	73.4
Tropical savannahs and grasslands	16.0	12.2	22.1
Temperate grasslands and shrublands	41.3	32.8	54.6
Deserts	36.3	27.6	49.9
Tundra	65.2	44.7	78.0
Croplands	22.1	17.0	30.1
Wetlands	19.7	15.2	26.7
Total	22.5	18.1	29.4

Total ecosystem turnover times of carbon per biome, estimated using equation (1) and stocks and fluxes aggregated per biome. Data estimates of τ were aggregated by biomes defined previously (Extended Data Table 1), and the ranges reported are the 2.5th (P 2.5) and 97.5th (P 97.5) percentiles from the ensemble of τ estimates, which can be interpreted as the confidence intervals in these estimates. The total represents the global τ including all biomes.

Turnover times vary considerably with latitude, ranging from 255 yr (mean τ above 75° N) in the high northern latitudes to 15 yr in the equatorial tropics (Fig. 2a). We find that the most rapid latitudinal changes exist between the sub-Arctic zones and the temperate zones, and near the tropical circles (between 20 and 40° N). Within the tropics (between 20° N and 20° S), the variations in τ are comparatively minor. In the Northern Hemisphere, in the transition zone between 50 and 65° N, the spatial covariation of τ is strongest with temperature, but south of 50° N precipitation is the dominant associated variable (until the Equator and below 40° S (Fig. 2c, d, in blue)). Across all latitudes, higher precipitation is associated with shorter residence times (negative partial correlations), whereas correlations between τ and temperature are more variable across latitudes, being low in the northern tropical zone and

also north of 60° N. Overall, across the latitudinal range, the spatial correlations of τ with temperature and precipitation are significant, but only low to moderately so. We note that carbon turnover in ecosystems will depend on the time-integrated effect of climate variables and summary statistics, and that mean total precipitation and mean temperature can serve only as simple proxies.

The significance of soil organic carbon stocks in explaining the spatial variability of τ is pervasive (Extended Data Fig. 5b). For approximately 80% of the land surface, τ covaries more strongly with soil carbon stocks than with vegetation carbon stocks. However, the residence times of carbon in terrestrial ecosystems should tend to increase with vegetation longevity, and with allocation towards woody biomass. Hence, we expected extensive positive correlations of τ with tree cover. Nevertheless, we also find negative correlations (Extended Data Fig. 5a). Precipitation, which is associated with tree cover, could overshadow the tree effect by increasing turnover times disproportionally, but the negative correlations persist even when we control for precipitation (Extended Data Fig. 6 and Supplementary Information Section 3). An increasing probability of fire related to increasing fuel loads with above-ground biomass[20,21], thereby reducing turnover times, is a possible explanation for this apparent paradox. Others are the contribution of trees to wetter microclimates[22,23] and increasing nutrient availability[23,24] in regions of low tree density and transition regions. Additionally, other factors like natural and anthropogenic disturbances[25] or management activities[26] can accelerate rates of turnover and, consequently, reduce mean residence times.

We calculated the turnover times of carbon (equation (1) in models from the Coupled Model Intercomparison Project Phase 5 (CMIP5)) (see Methods section on CMIP5 and Supplementary Information Section 5). The broad latitudinal patterns of τ in the CMIP5 ensemble (Fig. 2b) are consistent with the observations (Fig. 2a) (Pearson correlation coefficient, $r = 0.88$; $P < 0.0001$), but with a mean underestimation bias in the latitudinal profile of 47% (normalized average error). However, the zonal mean carbon turnover times vary by a factor of 2 to 40 across the analysed CMIP5 models (Fig. 2b). The models differ strongly with respect to correlations of τ with their (modelled) climate variables[27]. Across almost all latitudes, we find a range from positive to negative correlations for both temperature and precipitation. In the Northern Hemisphere, model-derived correlations with temperature tend to be more negative than the observation-derived correlations[27] (Fig. 2c). For latitudes below 50° N, the model-derived correlations with precipitation are more positive when compared with the observation-derived correlations (Fig. 2d). In the tropical zones, the CMIP5 ensemble predicts increasing turnover times associated with higher precipitation, which contrasts with the observation-derived estimates.

Overall, the CMIP5 models correlate with the observation-derived estimates of τ ($r^2 = 0.38$, $P < 0.001$), but exhibit shorter turnover times (Fig. 3); this is reflected also in the global turnover times (~36% lower; Extended Data Table 2). The bias is particularly pronounced in the high northern latitudes and in the seasonally dry biomes of northern tropical Africa, North America, central southern Asia and east Australia. An underestimation of turnover times in the high latitudes can potentially be

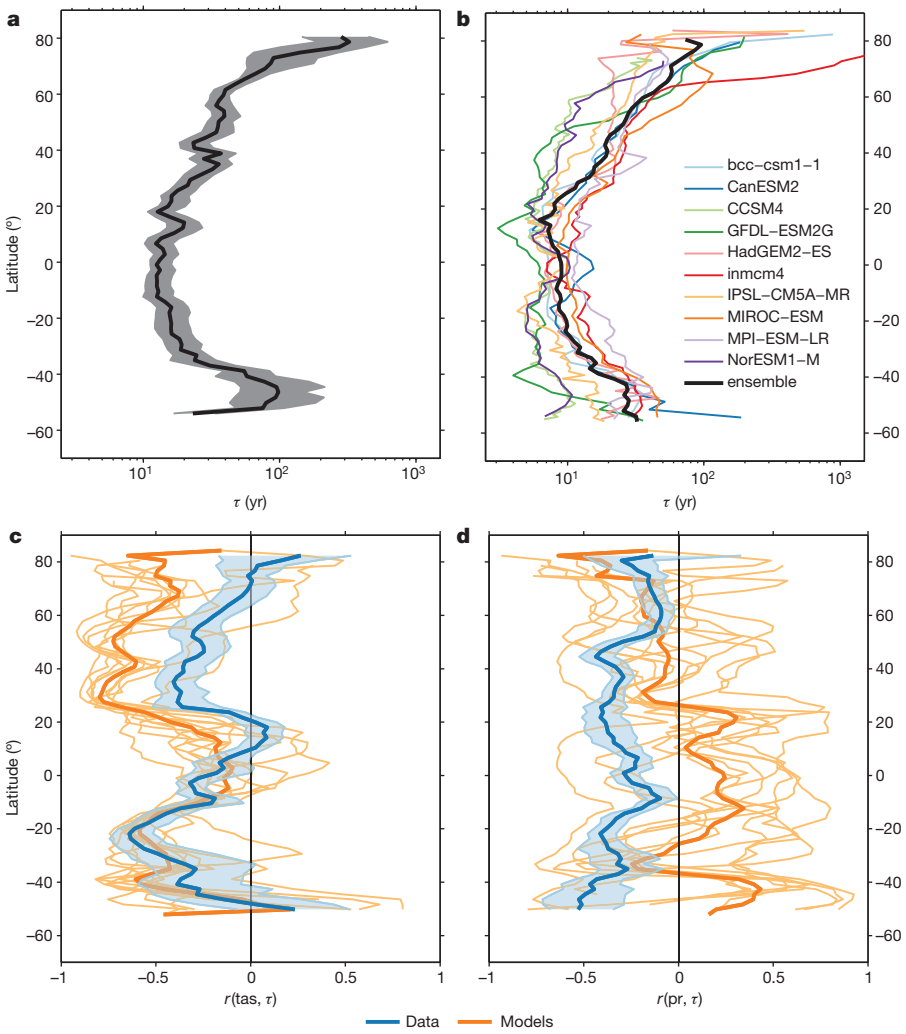

Figure 2 | Latitudinal gradients of whole ecosystem turnover times of carbon and associations to temperature and precipitation from data and models. Evaluation of latitudinal patterns and climate association of τ for data and models. The latitudinal gradients in τ from data (**a**) and from models (**b**) show distinctive associations with temperature (tas, **c**) and precipitation (pr, **d**). For consistency, the temperature and precipitation data sets considered for the model analysis are also model outputs (Methods section on CMIP5). The comparisons are based on partial correlations, controlling for precipitation when evaluating the association of τ with temperature (and vice versa), and are performed at the spatial scale of the NorESM1-M model output, to minimize artefacts in the correlations caused by differences in spatial resolution.

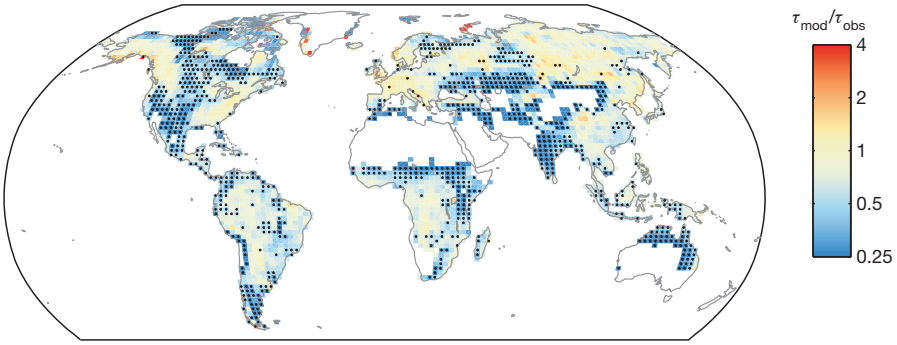

Figure 3 | Biases in whole-ecosystem carbon turnover times between models (τ_{mod}) and observation-derived (τ_{obs}) data ensembles. Stippling indicates locations where fewer than one-quarter of the models are within the 5th and 95th percentiles of the data. Here the deserts are filtered out according to a Köppen–Geiger classification (Extended Data Table 2) and to a minimum GPP of 10 gC m^{-2} yr^{-1}. The missing regions in southern Australia and New Zealand are due to missing data in the vegetation carbon data set (see Methods).

explained by either neglecting, or having an incomplete representation of, permafrost processes[28,29], although this can only partly explain differences in biases between North America and Siberia. Globally, in 31% of the land grid (35% of the global land area analysed), fewer than one-quarter of the models are within the confidence intervals of the data. Even assuming a 50% error in the observed carbon stocks and, consequently, in turnover times, this would not explain modelled turnover times differing by more than a factor of two from observations. Furthermore, despite representing soil organic carbon pools with long residence times, CMIP5 models do not provide an explicit representation of soil organic carbon vertical profiles. This could partly explain the observed differences but not the systematic underestimation of soil organic carbon up to 1 m depth in northern latitudes (Extended Data Fig. 7), which warrants attention to the representation of soil organic pools and vertical profiles in models.

Biases in simulated climate may also lend significant biases to model estimates of τ, although a comparison of differences in τ and spatial covariations with climate reveals that models fall short in describing the climate responses seen in the observation-derived data (Supplementary Information Section 6). Other possible reasons for this pronounced model bias may include responses to, or biases in, modelled soil moisture[27] or insufficient sensitivity of decomposition to drought. Moreover, adaptation of vegetation to dry conditions includes leaf sclerophylly, long leaf lifespans and higher wood densities in shrubs, which together lead to increased turnover times. In addition, interactions with nutrient cycles (for example that of nitrogen) may slow the turnover of carbon in ways which are not represented in models[30]. The spatial analysis shown here does not imply that the relationships between τ and climate factors are the same in the temporal dimension: these relationships emerge from the effects of climate—and other factors—through time, to which models should be comparable. In this regard, the emergence of appropriate model–data integration frameworks is essential for a consistent transfer of information from observation-based estimates of τ to modelling approaches[31].

We have presented an observation-based estimate of the total terrestrial carbon pool size and whole-ecosystem carbon turnover times and its spatial variation at 0.5° resolution with associated uncertainties. Our findings suggest significant hydrological control of carbon turnover, probably as relevant as temperature, adding to the well-known coupling between carbon and water cycling for photosynthesis, and calling for a better understanding of changes with the hydrological cycle. Although the ensemble mean of state-of-the-art coupled climate/carbon-cycle models reproduces the temperature-driven latitudinal patterns of carbon turnover times, we note an important underestimation bias and differences between models of more than one order of magnitude. The pronounced underestimation of whole-ecosystem carbon turnover times in semi-arid regions calls for a more accurate description of hydrological processes and water–carbon interactions. We expect that improved representations of the adaptation of vegetation to water availability, fire dynamics, and physicochemical and microbial soil organic carbon stabilization mechanisms[32], in addition to permafrost dynamics, will probably help to address the aforementioned biases. Overall, these results emphasize the role of water on the carbon dynamics in the terrestrial biosphere and suggest that future climate/carbon-cycle feedbacks will be more sensitive to changes in the water cycle than expected and represented in state-of-the-art models.

Online Content Methods, along with any additional Extended Data display items and Source Data, are available in the online version of the paper; references unique to these sections appear only in the online paper.

Received 9 November 2013; accepted 30 July 2014.
Published online 24 September 2014.

1. Friedlingstein, P. *et al.* Climate-carbon cycle feedback analysis: results from the (CMIP)-M-4 model intercomparison. *J. Clim.* **19,** 3337–3353 (2006).
2. Ciais, P. *et al.* in *Climate Change 2013: The Physical Science Basis* (eds Stocker, T. F. *et al.*) 465–570 (Cambridge Univ. Press, 2013).
3. King, A. W., Post, W. M. & Wullschleger, S. D. The potential response of terrestrial carbon storage to changes in climate and atmospheric CO_2. *Clim. Change* **35,** 199–227 (1997).
4. Sitch, S. *et al.* Evaluation of ecosystem dynamics, plant geography and terrestrial carbon cycling in the LPJ dynamic global vegetation model. *Glob. Change Biol.* **9,** 161–185 (2003).
5. Trumbore, S. Age of soil organic matter and soil respiration: radiocarbon constraints on belowground C dynamics. *Ecol. Appl.* **10,** 399–411 (2000).
6. Friend, A. D. *et al.* Carbon residence time dominates uncertainty in terrestrial vegetation responses to future climate and atmospheric CO_2. *Proc. Natl Acad. Sci. USA* **111,** 3280–3285 (2014).
7. Denman, K. L. *et al.* in *Climate Change 2007: The Physical Science Basis* (eds Solomon, S. *et al.*) 499–587 (Cambridge Univ. Press, 2007).
8. Heimann, M. & Reichstein, M. Terrestrial ecosystem carbon dynamics and climate feedbacks. *Nature* **451,** 289–292 (2008).
9. Anav, A. *et al.* Evaluating the land and ocean components of the global carbon cycle in the CMIP5 earth system models. *J. Clim.* **26,** 6801–6843 (2013).
10. Rodhe, H. in *Global Biogeochemical Cycles* (eds Charlson, R. J., Butcher, S. S., Orians, G. H. & Wolfe, G. V.) Ch. 4 (Academic, 1992).
11. Malhi, Y., Saatchi, S., Girardin, C. & Aragão, L. E. O. C. in *Amazonia and Global Change* (eds Keller, M., Bustamante, M., Gash, J. & Silva Dias, P.) 355–372 (American Geophysical Union, 2009).
12. Trumbore, S. Carbon respired by terrestrial ecosystems — recent progress and challenges. *Glob. Change Biol.* **12,** 141–153 (2006).
13. Sundquist, E. T. in *The Carbon Cycle and Atmospheric CO: Natural Variations, Archean to Present* (eds Sundquist, E. T. & Broecker, W. S.) 5–59 (American Geophysical Union, 1985).
14. Kätterer, T., Reichstein, M., Andren, O. & Lomander, A. Temperature dependence of organic matter decomposition: a critical review using literature data analyzed with different models. *Biol. Fertil. Soils* **27,** 258–262 (1998).
15. Davidson, E. A. & Janssens, I. A. Temperature sensitivity of soil carbon decomposition and feedbacks to climate change. *Nature* **440,** 165–173 (2006).
16. Bond-Lamberty, B. & Thomson, A. Temperature-associated increases in the global soil respiration record. *Nature* **464,** 579–582 (2010).
17. Cleveland, C. C. & Townsend, A. R. Nutrient additions to a tropical rain forest drive substantial soil carbon dioxide losses to the atmosphere. *Proc. Natl Acad. Sci. USA* **103,** 10316–10321 (2006).
18. Houghton, R. A. Revised estimates of the annual net flux of carbon to the atmosphere from changes in land use and land management 1850–2000. *Tellus B* **55,** 378–390 (2003).
19. Nepstad, D. C. *et al.* Large-scale impoverishment of Amazonian forests by logging and fire. *Nature* **398,** 505–508 (1999).
20. Thonicke, K., Venevsky, S., Sitch, S. & Cramer, W. The role of fire disturbance for global vegetation dynamics: coupling fire into a dynamic global vegetation model. *Glob. Ecol. Biogeogr.* **10,** 661–677 (2001).
21. Krawchuk, M. A. & Moritz, M. A. Constraints on global fire activity vary across a resource gradient. *Ecology* **92,** 121–132 (2011).
22. Vetaas, O. R. Micro-site effects of trees and shrubs in dry savannas. *J. Veg. Sci.* **3,** 337–344 (1992).

23. Joffre, R. & Rambal, S. How tree cover influences the water-balance of Mediterranean rangelands. *Ecology* **74,** 570–582 (1993).
24. Belsky, A. J. Influences of trees on savanna productivity — tests of shade, nutrients, and tree-grass competition. *Ecology* **75,** 922–932 (1994).
25. Fahey, T. J. *et al.* The biogeochemistry of carbon at Hubbard Brook. *Biogeochemistry* **75,** 109–176 (2005).
26. Bondeau, A. *et al.* Modelling the role of agriculture for the 20th century global terrestrial carbon balance. *Glob. Change Biol.* **13,** 679–706 (2007).
27. Todd-Brown, K. E. O. *et al.* Causes of variation in soil carbon simulations from CMIP5 Earth system models and comparison with observations. *Biogeosciences* **10,** 1717–1736 (2013).
28. Vonk, J. E. & Gustafsson, O. Permafrost-carbon complexities. *Nature Geosci.* **6,** 675–676 (2013).
29. Koven, C. *et al.* On the formation of high-latitude soil carbon stocks: Effects of cryoturbation and insulation by organic matter in a land surface model. *Geophys. Res. Lett.* **36,** L21501 (2009).
30. Janssens, I. A. *et al.* Reduction of forest soil respiration in response to nitrogen deposition. *Nature Geosci.* **3,** 315–322 (2010).
31. Xia, J. Y., Luo, Y. Q., Wang, Y. P. & Hararuk, O. Traceable components of terrestrial carbon storage capacity in biogeochemical models. *Glob. Change Biol.* **19,** 2104–2116 (2013).
32. Wieder, W. R., Bonan, G. B. & Allison, S. D. Global soil carbon projections are improved by modelling microbial processes. *Nature Clim. Change* **3,** 909–912 (2013).

Supplementary Information is available in the online version of the paper.

Acknowledgements We would like to thank C. Jones for comments that improved the manuscript. We are grateful to A. Ito, D. Zaks and S. Del Grosso for sharing their NPP data sets with us. We thank S. Schott for figure editing. We acknowledge support by the European Union (FP7) through the projects GEOCARBON (283080), CARBONES (242316) and EMBRACE (283201) and an ERC starting grant QUASOM (ERC-2007-StG-208516).

Author Contributions N.C. and M.R. designed the study and are responsible for the integrity of the work as a whole. N.C., M.F. and M. Migliavacca performed analysis and calculations. N.C. and M.R. mainly wrote the manuscript. M.K. and J.B. contributed to interpreting and processing the soil databases. M.T., M.S. and S.S. contributed to the vegetation carbon stocks datasets and interpretation. M.J. contributed to the GPP datasets and interpretation. C.B., M. Mu, M.T. and U.W. contributed to data provision, analysis or data processing. A.C., B.A., M.F., M.J. and J.T.R. contributed to analysis design and interpretation. All authors discussed and commented on the manuscript.

Author Information Reprints and permissions information is available at www.nature.com/reprints. The authors declare no competing financial interests. Readers are welcome to comment on the online version of the paper. Correspondence and requests for materials should be addressed to N.C. (nuno.carvalhais@bgc-jena.mpg.de).

METHODS

Estimates of total soil organic carbon based on global databases. The Harmonized World Soil Database[33] condenses a comprehensive collection of geographic information on soil physical and chemical properties from regional and national inventories all over the world. The HWSD is organized in mapping units, each consisting of particular combinations of different soils referred to as 'soil ID' from here on. For every soil ID, among other variables, the database reports texture, bulk density and concentration of organic carbon for the top (0 to 10 or 30 cm) and subsoil (from 30 cm to 1 m depth) layers. Estimates of total organic carbon for each soil ID can then be computed per layer as follows:

$$\mathrm{SOC} = \frac{\mathrm{OC}}{100} D \left(1 - \frac{G}{100}\right) \mathrm{BD}$$

Here soil organic carbon stocks (SOC, kg C m^{-2}) is estimated from organic carbon content (OC, wt%), layer thickness (D, m), gravel content (G, vol%) and bulk density (BD, kg m^{-3}). Such an approach allows for estimates of SOC in the top layer (0–30 cm) and in the subsoil layer (30–100 cm). We used these two estimates to fit two empirical models of cumulative SOC (equations (2) and (3)), which were then integrated until the full soil depth (D_f) per soil ID was reached, as follows:

$$\log(\mathrm{SOC}) = K \log(D) + I \quad (2)$$

$$\mathrm{SOC} = a \log(Db + 1) \quad (3)$$

Here K, I, a and b are empirical parameters estimated per soil ID. Estimates using equation (2) follow ref. 34 for the model with the least mean predictive error (see table 1 in ref. 34). Additionally, on the basis of *in situ* observations of SOC (ref. 35), we included an alternative model formulation that has shown a strong fit to data, as well as a faster saturation of cumulative SOC with depth (Supplementary Fig. 1). Here the latter model represents a more conservative estimation of full-depth SOC.

The full depth of the soil (D_f) was extracted from the Global Soil Texture And Derived Water-Holding Capacities database[36]. This database contains standardized values of soil depth and textures for the globe, which were selected for the same soil types in the same continents, according to continents defined in ref. 37.

The HWSD was still a work in progress at the time of our study, such that data from certain regions in the world still needed updating and were therefore considered less reliable. Two such regions were North America and northern Eurasia[33]. Therefore, as an alternative to the HWSD, we also considered the Northern Circumpolar Soil Carbon Database[38,39] (NCSCD) in our SOC estimates for northern latitudes[38,39]. We generated a set of global SOC estimates, which included factorial combinations of SOC from the HWSD, extrapolated to full soil depth using both empirical models, and also used the NCSCD data set for northern latitudes. These data sets were aggregated from ~1 km^2 (0.01° by 0.01°) to ~55 km^2 (0.5° by 0.5°) resolution. Our global estimate of total soil organic carbon was $2{,}397^{+860}_{-561}$ PgC (mean; upper limit, percentile 97.5; lower limit, percentile 2.5) (Supplementary Fig. 2). The global soil carbon stocks are comparable to a previous estimate of total soil organic carbon of 2,344 PgC in the top 3 m of soil[34] (Supplementary Table 1). The range of estimated SOC values varied significantly between the different biome types across the world (Supplementary Table 1). According to our estimates, tropical biomes (forest, savannahs, grasslands) together account for 32% of the global soil carbon stock, and the areas of largest integrated stock are found in tropical (20%) and boreal (19%) forests.

A comprehensive assessment of the uncertainties in the SOC estimates should integrate the uncertainties from several sources: from (1) the uncertainties in the soil profiles and depth information to (2) uncertainties in the spatial extrapolation to a global extent, including (3) uncertainties in the extrapolation to full depth and (4) those emerging from the different data sources considered here (the HWSD and the NCSCD). The ability to quantify the uncertainties stemming from all these sources, and propagate them to the final SOC estimates, is limited by the available information. But here we are able to explicitly propagate the uncertainties that stem from the methods used to extrapolate SOC to full depth (from both the aforementioned empirical models; equations (2) and (3)) and from the different data sources (HWSD and NCSDC), by creating individual SOC estimates, which are combined individually with the estimates of vegetation stocks and GPP for explicit propagation of the uncertainties in τ. The quantification of the uncertainties in the total SOC stemming from depth are propagated by exploring the variability present in the soil depth from the WISE data set for the same soil types as in the HWSD. We do so by contrasting soil depth standard deviations against soil depth ($\sigma_{Df} = 0.19 D_f$; $r = 0.28$, $P < 10^{-10}$, $N = 4{,}790$), for which we draw additionally 50 random samples of depth (with a σ_{Df} of 19%) to estimate the uncertainties in total SOC that may stem from the soil depth considered.

Overall, this approach is based on the best available information, and addresses uncertainties by evaluating the spread in the generated ensembles. We acknowledge that the integration of uncertainties stemming from the soil profiles and depth, and from the regionalization to the global scale, could alter the uncertainties presented here. The provision of information on these sources of uncertainty, and the ability to tackle them in future estimates is essential to a more comprehensive assessment of data uncertainty.

Deriving total vegetation carbon. Our global estimates of total vegetation carbon were derived from a collection of estimates for pan-tropical regions[40] and for northern and temperate forests[41] based on radar remote-sensing retrievals[42]. Above- and below-ground biomass uncertainty for the tropical regions was propagated from errors in measurements, allometric relations, sampling and predictions[40]. In the Northern Hemisphere, estimates accounted for uncertainties in the BIOMASAR GSV data, wood density data and biomass compartment data[41]. On regional scales, the Northern Hemisphere biomass map in comparison with inventory-based data showed strong agreement (Russia: $r^2 = 0.78$ and NRMSE = 0.35; United States: $r^2 = 0.90$ and NRMSE = 0.32; Europe: $r^2 = 0.70$ and NRMSE = 0.40; NRMSE denotes the root mean squared error divided by the mean of the observations) and can thus be considered a very suitable product at 0.5° resolution. Evaluation results for the United States and Europe have shown that this data set might slightly underestimate high carbon densities due to the use of C-band radar data, but there was no systematic error detected in the intercomparison in Russia[41].

One shortcoming of the above two products is the sole consideration of tree forms in their estimates. Therefore, to account for the herbaceous biomass in our estimates, we assumed a mean turnover time of one year in the live vegetation fraction per grid cell, and, given that the costs of autotrophic respiration vary significantly[43], we took the respiratory costs (α) to lie in the range 25%–75% (uniformly distributed):

$$C_H = \mathrm{GPP}(1 - \alpha) f_H$$

Here C_H is the herbaceous component of carbon in vegetation; GPP is the gross primary production, based on the newest data driven estimates[44]; α is the respiration cost; and f_H is the fraction of each 0.5° grid cell considered as herbaceous in the SYNMAP[45]. The correlation (r^2) between the data set accounting for non-woody stocks and the original vegetation stock estimates was 0.98 ± 0.015, and the normalized mean absolute error was 0.07.

By accounting for herbaceous cover in our global C stock estimates, we obtained differences of less than 1% in the mean global τ, with the highest differences observed for croplands (1.3%), temperate grasslands and shrublands (0.6%), and wetlands (0.6%). Therefore, accounting for herbaceous plants in our global carbon stocks did not make much of a difference to the final estimates of τ. We note that these differences may not fully reflect the dynamics in natural vegetation types, which may include below-ground perennial roots or rhizomes. However, even a threefold increase in vegetation mean residence times of carbon would result in a difference of less than 2% in total ecosystem turnover times globally. These results reflect the large contribution of woody vegetation and, mostly, of soil organic carbon to the global carbon stock estimates. Overall, terrestrial vegetation holds about 442 ± 146 PgC (mean ± standard deviation), which is ~16% of the global organic carbon estimated on land (Supplementary Table 2). Excluding herbaceous vegetation, our estimate of 429 ± 144 PgC in forests encompasses the latest rounded estimate of 300 PgC derived from global inventory data[46]. The most significant part of vegetation carbon is found in tropical forests and tropical savannahs and grasslands (62%), and temperate and boreal forests, and temperate grasslands and shrublands incorporate circa 25%.

Global carbon estimates. The ensemble of vegetation carbon pools was composed of 200 members, assuming normally distributed uncertainties in the satellite-derived C stocks and in GPP estimates, and a uniform distribution of autotrophic respiration costs (see previous Methods section). Each member of the ensemble of total soil carbon was individually added to each of the members of vegetation carbon ensemble. We randomly sampled 200 members of this ensemble to achieve the final data ensemble of total ecosystem carbon stocks (Fig. 1a) with uncertainties (Extended Data Fig. 1). The uncertainty bands in the latitudinal profiles in Extended Data Fig. 7 report the 5th and 95th percentiles of the data ensemble per latitudinal window.

Global mean turnover times of carbon. Turnover time is commonly defined as the ratio between the total size of a reservoir and its outflux[47]. For terrestrial ecosystems, the total reservoir size is equal to the carbon stock in vegetation and soils, and the outflux comprises all carbon losses (respiration of autotrophic plants, respiration of heterotrophic organisms, losses by fire and harvest). Under the assumption that the ecosystem is neither gaining nor loosing carbon (steady state), the turnover time can equivalently be calculated as the ratio between the carbon stock in vegetation (C_{veg}) and soils (C_{soil}), and the flux into this reservoir, GPP:

$$\tau = \frac{C_{veg} + C_{soil}}{\mathrm{GPP}} \quad (4)$$

In steady state, τ is the average time that newly assimilated carbon spends in terrestrial ecosystems before it is respired, burnt or harvested. Acknowledging that our definition of τ (equation (4)) hinges on the steady-state assumption, we call τ the

apparent whole-ecosystem turnover time and interpret the quantity as an emergent diagnostic at ecosystem level (Supplementary Information Section 1). An ensemble of apparent whole-ecosystem turnover times (τ) was obtained by applying equation (1) to a random permutation of the mean annual GPP (1982–2005) and total ecosystem carbon data sets ($N = 200$). The resulting uncertainties had wide ranges in space (Supplementary Fig. 3) and between biomes (Table 1). The uncertainty bands in the latitudinal profiles in Fig. 2a report the 5th and 95th percentiles of data ensemble per latitudinal window.

Benchmarking our current results against other observation-based estimates of global carbon turnover time is hampered by the fact that previous studies have mostly focused on soils. Global turnover times of carbon in soils were reported to range from 27 yr (ref. 48) to 32 yr (ref. 49), and were generally considered to lie between 30 and 40 yr, assuming strong variations for different ecosystems[50]. The spatial variations in the residence times of carbon in soils also reflect climate controls, exhibiting longer residence times in cold biomes at high latitudes (as shown in ref. 51 using ^{14}C for forest soils). Such spatial variations are also seen in τ (Fig. 1a), which shows a latitudinal range from 255 yr in high northern latitudes (mean τ north of 75° N) to 15 yr in the equatorial tropics (Fig. 2a). In ref. 13, several estimates of global NPP (table 13), soil organic carbon (table 14) and vegetation stocks (table 12) were reported. Assuming respiration costs of around 50%, whole-ecosystem turnover time can be estimated as $\tau = C_{total}/(NPP + RA)$ (RA, autotrophic respiration). By combining the different quantities of stocks and fluxes, a global τ of 21 ± 7 yr (mean $\pm$ standard deviation) can be estimated.

For model evaluation, the separation between the soil and vegetation components of τ is useful for a more detailed diagnostic of model performance. We define τ_{soil} as the ratio between C_{soil} and net primary production (NPP) and τ_{veg} as the ratio between C_{veg} and GPP. However, the spatial representation of observation-based empirical estimates of NPP is still hampered by the difficulty of accounting for autotrophic respiration fluxes. Hence, the confidence level for NPP spatial estimates (for example, from ref. 52) still falls short to the levels of GPP estimates[44]. An approach is to consider an ensemble of NPP fields supported by observation-based empirical estimates based on climate patterns. A set of state-of-the-art global NPP fields from refs 52–57 is used to build a data-driven empirical ensemble. Each of these NPP fields is combined individually with the C_{soil} ensemble members to build an ensemble of τ_{soil} for comparison to the CMIP5 model results. For the construction of τ_{veg} ensemble, we relied on the GPP and vegetation carbon stocks described above.

The data used here can be obtained from http://www.bgc-jena.mpg.de/geodb/BGI/tau.php.

Climate data. Climate data are based on the European Centre for Medium-Range Weather Forecasts (ECMWF) ERA-Interim reanalysis product[58] and have been bias-corrected as described in ref. 59. We obtained daily data with a grid cell size of 0.5° during 1979–2010 from ECMWF. This reanalysis data was bias-corrected against the WATCH forcing data[60] using an overlapping period of 1979–2001 and following the standard procedure[61]. Ideally, this approach conserves statistical moments of the distribution, for example the mean and variance. In addition, the number of rainy days remains unchanged. The WATCH forcing data serves as the reference data set because it has already been bias-corrected against other climatic data sets[60]. For the analysis, we computed the mean fields of each of the climate variables by averaging the whole data sets per grid cell between 1982 and 2005.

Correlation analysis. The association between τ and climate is assessed locally for each grid cell of the global data sets by computing local correlations using a 5.5°-by-5.5° moving window (11 by 11 grid cells). This approach enables the assessment of the local importance of climate factors (Supplementary Information Section 2) and yields a global estimate of regional covariation of τ with climate variables—temperature and precipitation. The association between τ and climate is determined by analysing the Pearson correlation, partial correlation coefficients and the non-parametric Spearman's rank correlation coefficient. To disentangle the relative importance of temperature and precipitation in determining the spatial patterns of τ, we (1) used the Lindeman–Merenda–Gold (LMG) method[62], implemented in ref. 63, which allows to quantify the contribution of different correlated regressors (here temperature and precipitation) to a multiple linear regression model; and (2) quantified the changes in the residual sums of squares by removing each independent variable from a bivariate regression between temperature and precipitation: $RI_v = (RSS_v - RSS_{tas,pr})/TSS$, where RI_v is the relative importance of variable v, RSS_v is the residual sum of squares of the regression of τ with variable v, $RSS_{tas,pr}$ is the residual sum of squares of the regression of τ against temperature and precipitation, and TSS is the total sum of squares. Finally, the metrics (RI_{tas} and RI_{pr}) are normalized (divided by r^2) to sum to 1 (ref. 63). In addition, we performed a conditional independence test on rejecting the null hypothesis that τ is independent of precipitation or temperature given the dependence on temperature or, respectively, precipitation[64]. Latitudinal correlations between τ and climate variables are based on partial correlation coefficients between τ and temperature or precipitation, controlling for precipitation or, respectively, temperature. The analysis is conducted on a common grid size for the CMIP5 models (see next section) and the observation-derived τ and climate for a latitudinal window of ~9.5° (5 grid cells). Partial correlations are computed individually for each ensemble member of the data and the models. The uncertainty bands in the data ensemble (Fig. 2c, d) represent the 5th and 95th percentiles of the partial correlations per latitudinal window.

Processing Earth system model outputs from CMIP5. We analysed historical simulations outputs from ten Earth system models from CMIP5[65] (Supplementary Table 3). The historical scenario simulations (also known as the 20th-century simulations) for CMIP5 were carried out for the period from the start of the industrial revolution to near present: 1850–2005. The Earth system model here is the atmosphere–ocean coupled global climate model coupled to a carbon-cycle model, and was forced in diagnostic mode by observed changes in atmospheric composition from natural and anthropogenic sources, volcanoes, greenhouse gases and aerosols, as well as changes in solar output and land cover. The model outputs evaluated relate to climate (temperature (tas), precipitation (pr), net and shortwave downward radiation (Rn and rsds, respectively)); carbon fluxes (net ecosystem exchange (nee), gross primary production (gpp), net primary production (npp) and autotrophic and heterotrophic respiration fluxes (ra and rh, respectively) to determine ecosystem respiration (reco = ra + rh); and carbon pools (accounting for leaf (cLeaf), wood (cWood) and roots (cRoot) in vegetation; and accounting for soil (cSoil), litter (cLitter) and woody debris (cCwd) in soil).

The spatial fields of the variables were obtained by computing mean annual values between 1982 and 2005. The ranges stand for the common period between data availability for GPP fluxes[44] and the historical runs from CMIP5. Like for the data, the modelled values of τ are estimated from equation (1) using these simulation outputs.

Model outputs were always processed at the native spatial resolutions. To perform comparisons between models and between models and data, we constructed a common grid model ensemble. The common model ensemble was built by aggregating all model outputs to a common spatial grid, corresponding to the resolution of the NorESM1-M model (~1.89° by 2.5°, latitude by longitude). The aggregation consisted of computing an area-weighted mean per grid cell. Because each model shows a different number of model realizations (number of model ensembles in Supplementary Table 3), we averaged all ensembles per model to avoid overweighting models with a higher number of realizations. The original grid outputs were used for within-model evaluations (partial correlations, latitudinal gradients, global and biome statistics).

33. FAO/IIASA/ISRIC/ISSCAS/JRC. *Harmonized World Soil Database v 1. 2* http://webarchive.iiasa.ac.at/Research/LUC/External-World-soil-database/HTML/ (2012).
34. Jobbágy, E. G. & Jackson, R. B. The vertical distribution of soil organic carbon and its relation to climate and vegetation. *Ecol. Appl.* **10,** 423–436 (2000).
35. Schrumpf, M., Schulze, E. D., Kaiser, K. & Schumacher, J. How accurately can soil organic carbon stocks and stock changes be quantified by soil inventories? *Biogeosciences* **8,** 1193–1212 (2011).
36. Webb, R. W., Rosenzweig, C. E. & Levine, E. R. *Global Soil Texture and Derived Water-Holding Capacities (Webb et al.)* http://daac.ornl.gov/cgi-bin/dsviewer.pl?ds_id=548 (Oak Ridge National Laboratory Distributed Active Archive Center, 2000).
37. Zobler, L. *A World Soil File for Global Climate Modelling*. Report No. 87802 (NASA Goddard Institute for Space Studies, 1986).
38. Hugelius, G. *et al.* The Northern Circumpolar Soil Carbon Database: spatially distributed datasets of soil coverage and soil carbon storage in the northern permafrost regions. *Earth Syst. Sci. Data* **5,** 3–13 (2013).
39. Tarnocai, C. *et al.* Soil organic carbon pools in the northern circumpolar permafrost region. *Glob. Biogeochem. Cycles* **23,** GB2023 (2009).
40. Saatchi, S. S. *et al.* Benchmark map of forest carbon stocks in tropical regions across three continents. *Proc. Natl Acad. Sci. USA* **108,** 9899–9904 (2011).
41. Thurner, M. *et al.* Carbon stock and density of northern boreal and temperate forests. *Glob. Ecol. Biogeogr.* **23,** 297–310 (2014).
42. Santoro, M. *et al.* in *Proc. ESA Living Planet Symp.* SP-722 (CD-ROM, ESA Communication Office, 2013).
43. Amthor, J. S. The McCree-de Wit-Penning de Vries-Thornley respiration paradigms: 30 years later. *Ann. Bot. (Lond.)* **86,** 1–20 (2000).
44. Jung, M. *et al.* Global patterns of land-atmosphere fluxes of carbon dioxide, latent heat, and sensible heat derived from eddy covariance, satellite, and meteorological observations. *J. Geophys. Res. Biogeosci.* **116,** G00J07 (2011).
45. Jung, M., Henkel, K., Herold, M. & Churkina, G. Exploiting synergies of global land cover products for carbon cycle modeling. *Remote Sens. Environ.* **101,** 534–553 (2006).
46. Kauppi, P. E. New, low estimate for carbon stock in global forest vegetation based on inventory data. *Silva Fenn.* **37,** 451–457 (2003).
47. Rodhe, H. in *Global Biogeochemical Cycles* (eds Butcher, S. S., Charlson, R. J., Orians, G. H. & Wolfe, G. V.) 55–72 (Academic, 1992).
48. Jenkinson, D. S. in *Russell's Soil Conditions and Plant Growth* (ed. Wild, A.) 564–607 (Longman Scientific and Technical, 1988).
49. Schlesinger, W. H. in *Soils and Global Change* Vol. 25 (eds Lal, R., Kimble, J., Levine, E. & Stewart, B. A.) 9–25 (CRC/Lewis Publishers, 1995).

50. Oades, J. M. The retention of organic-matter in soils. *Biogeochemistry* **5,** 35–70 (1988).
51. Bird, M. I., Chivas, A. R. & Head, J. A latitudinal gradient in carbon turnover times in forest soils. *Nature* **381,** 143–146 (1996).
52. Ito, A. A historical meta-analysis of global terrestrial net primary productivity: are estimates converging? *Glob. Change Biol.* **17,** 3161–3175 (2011).
53. Zaks, D. P. M., Ramankutty, N., Barford, C. C. & Foley, J. A. From Miami to Madison: investigating the relationship between climate and terrestrial net primary production. *Glob. Biogeochem. Cycles* **21,** GB3004 (2007).
54. Del Grosso, S. *et al.* Global potential net primary production predicted from vegetation class, precipitation, and temperature. *Ecology* **89,** 2117–2126 (2008).
55. Lieth, H. in *Primary Productivity of the Biosphere* (eds Lieth, H. & Whittaker, R. H.) 237–263 (Springer, 1975).
56. Lieth, H. & Box, E. in *Publications in Climatology* (ed. Thornthwaite, W.) 37–46 (C.W. Thornthwaite Associates, 1972).
57. Schuur, E. A. G. Productivity and global climate revisited: the sensitivity of tropical forest growth to precipitation. *Ecology* **84,** 1165–1170 (2003).
58. Dee, D. P. *et al.* The ERA-Interim reanalysis: configuration and performance of the data assimilation system. *Q. J. R. Meteorol. Soc.* **137,** 553–597 (2011).
59. Beer, C. *et al.* Harmonized European long-term climate data for assessing the effect of changing temporal variability on land-atmosphere CO2 fluxes. *J. Clim.* **27,** 4815–4834 (2014).
60. Weedon, G. P. *et al.* Creation of the WATCH forcing data and its use to assess global and regional reference crop evaporation over land during the twentieth century. *J. Hydrometeorol.* **12,** 823–848 (2011).
61. Piani, C. *et al.* Statistical bias correction of global simulated daily precipitation and temperature for the application of hydrological models. *J. Hydrol. (Amst.)* **395,** 199–215 (2010).
62. Lindeman, R. H., Merenda, P. F. & Gold, R. Z. *Introduction to Bivariate and Multivariate Analysis* (1980).
63. Grömping, U. Relative importance for linear regression in R: the package relaimpo. *J. Stat. Softw.* **17,** 1–27 (2006).
64. Zhang, K., Peters, J., Janzing, D. & Schölkopf, B. Kernel-based conditional independence test and application in causal discovery. *Computing Res. Repos.* (arXiv, 2012).
65. Taylor, K. E., Stouffer, R. J. & Meehl, G. A. An Overview of Cmip5 and the Experiment Design. *Bull. Am. Meteorol. Soc.* **93,** 485–498 (2012).
66. Prentice, I. C. *et al.* in *Climate Change 2001: The Scientific Basis* (eds Houghton, J. T. *et al.*) 183–237 (Cambridge Univ Press, 2001).
67. Beer, C. *et al.* Terrestrial gross carbon dioxide uptake: global distribution and covariation with climate. *Science* **329,** 834–838 (2010).
68. Kottek, M., Grieser, J., Beck, C., Rudolf, B. & Rubel, F. World map of the Koppen-Geiger climate classification updated. *Meteorol. Z. (Berl.)* **15,** 259–263 (2006).
69. Turetsky, M. R. *et al.* The resilience and functional role of moss in boreal and arctic ecosystems. *New Phytol.* **196,** 49–67 (2012).
70. Page, S. E., Rieley, J. O. & Banks, C. J. Global and regional importance of the tropical peatland carbon pool. *Glob. Change Biol.* **17,** 798–818 (2011).
71. DiMiceli, C. M. *et al. Annual Global Automated MODIS Vegetation Continuous Fields (MOD44B) at 250 m Spatial Resolution for Data Years Beginning Day 65, 2000 - 2010, Collection 5 Percent Tree Cover* http://glcf.umd.edu/data/vcf/ (University of Maryland, 2011).

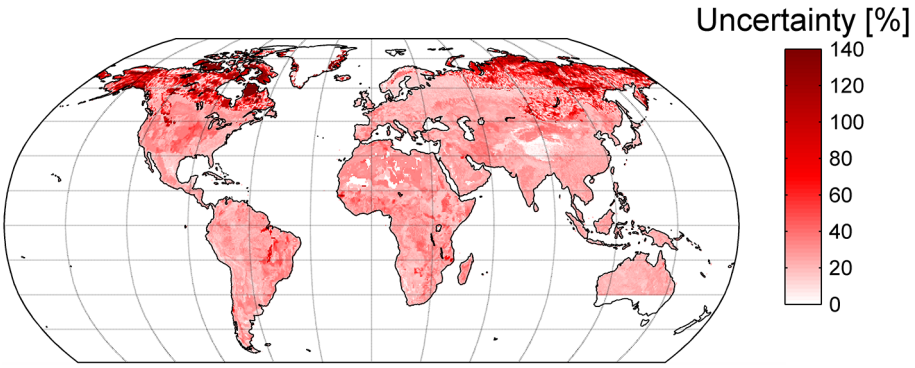

Extended Data Figure 1 | Relative uncertainties in total ecosystem carbon. Relative uncertainties in total ecosystem carbon stemming from the different data sources considered, reported as the ratio between the interquartile range (difference between the 75th and 25th percentiles) of the different estimates and the mean. The colour scale is binned to the 98th percentile of the spatial distribution of uncertainty (140%). A significant spatial variability was observed in the total ecosystem carbon uncertainties. The highest uncertainties locally and regarding total stocks per biome were observed in tundra (~38%), followed by tropical savannahs and grasslands (~30%). Deserts and croplands also showed significant relative uncertainties (both 27%). Overall, we observe a global relative uncertainty of 21%. We note unknown sources of uncertainties related to total carbon stocks, which relate mostly the representativeness of mosses in northern latitudes[69] and tropical peatlands in Southeast Asia, although we find a total soil stock of $\sim 83^{+31}_{-19}$ PgC (95% CI) in this region ($-11.5^{\circ} <$ latitude $< 10^{\circ}$ and $90^{\circ} <$ longitude $< 155^{\circ}$), which borders the upper envelope of the estimates in ref. 70.

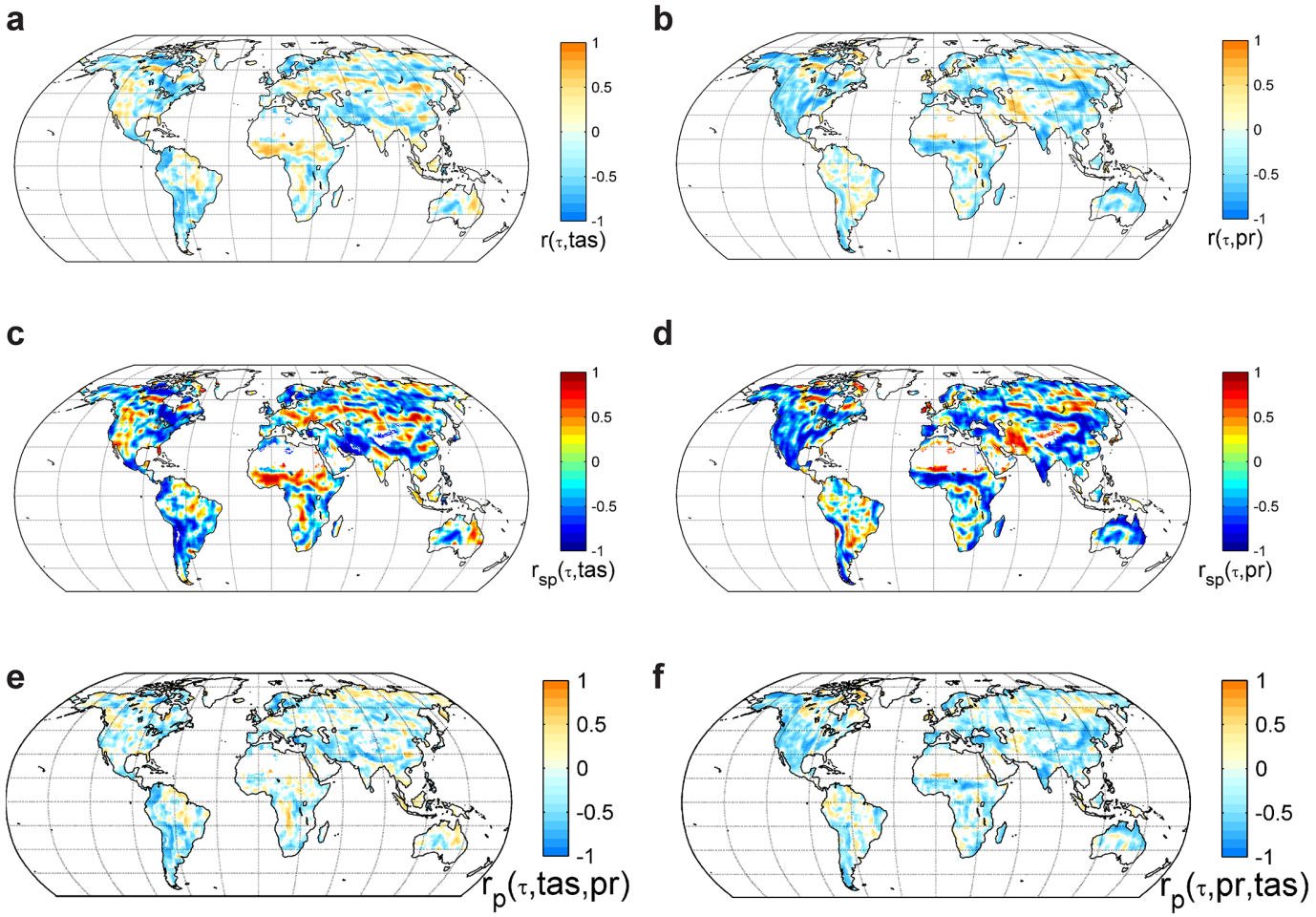

Extended Data Figure 2 | Local spatial correlations between turnover times of carbon in terrestrial ecosystems and temperature, and precipitation. Local spatial correlations between τ and temperature (tas; **a**, **c**, **e**), and τ and precipitation (pr; **b**, **d**, **f**) using the 5.5°-by-5.5° moving-window approach. We use two alternative approaches to the Pearson correlation (**a**, **b**): the Spearman rank correlation (r_{sp}), a non-parametric measure of association that does not rely on the assumption of normal distribution of residuals (**c**, **d**); and the partial correlation (r_p, **e**, **f**), measuring the degree of association between τ and temperature or precipitation, setting precipitation or, respectively, temperature as controlling variables (**e**, **f**). On local scales, using partial correlations may result in lost correlation owing to a strong local covariation of temperature and precipitation. Although we see this loss, the associative patterns between τ and both climate variables are generally maintained across the approaches used to calculate the correlations.

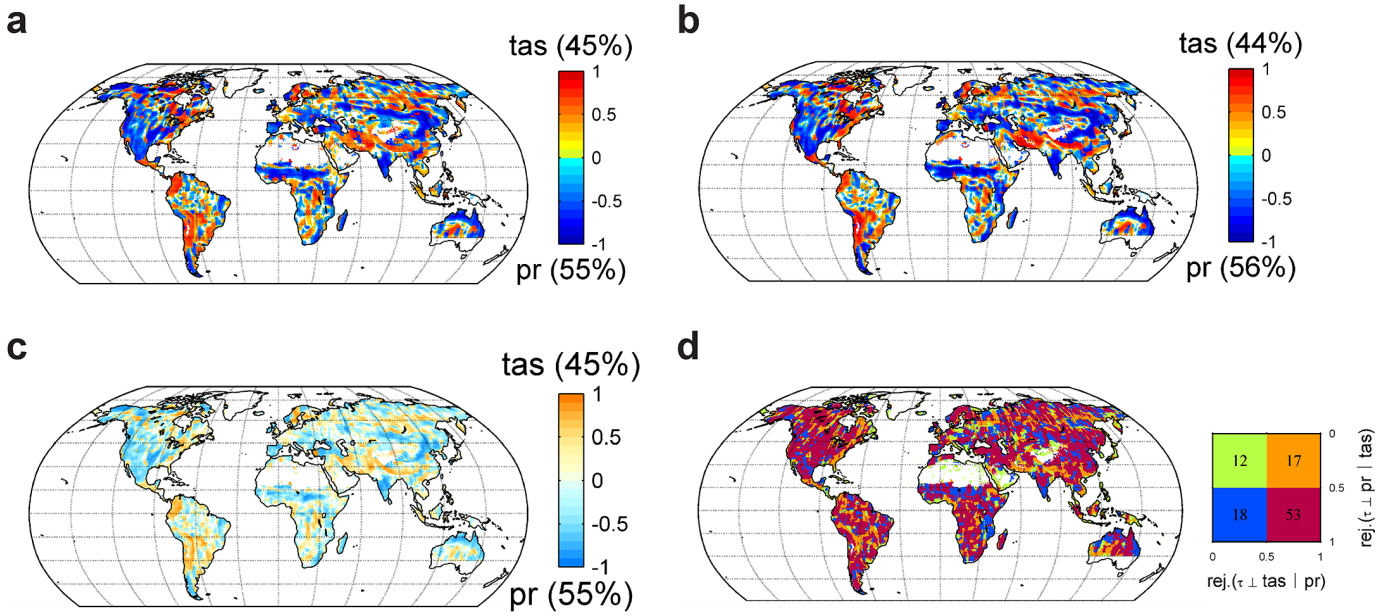

Extended Data Figure 3 | Strength of association between turnover times of carbon in terrestrial ecosystems and temperature, and precipitation, using different methods. Strength of association between τ and temperature (tas) and precipitation (pr) for Pearson correlations (**a**), Spearman correlations (**b**) and partial correlations (**c**). Each of these maps (**a**–**c**) shows regions where the association of τ is stronger with precipitation (blue) or temperature (red). The fraction of land grid cells with stronger significant correlations to temperature and precipitation are indicated above (for tas) and below (for pr) the colour bar. The colour gradients reflect the respective absolute correlation values. Despite stronger correlations with either temperature or precipitation, these cannot be said to be completely independent from the variable with lower correlation strength. **d**, Results of a conditional independence test on rejecting the null hypothesis that τ is independent from pr or tas given tas or, respectively, pr (ref. 64), showing that in 53% of the land grid cells, the dependence of τ on temperature or precipitation is not lost when controlling for precipitation or, respectively, temperature.

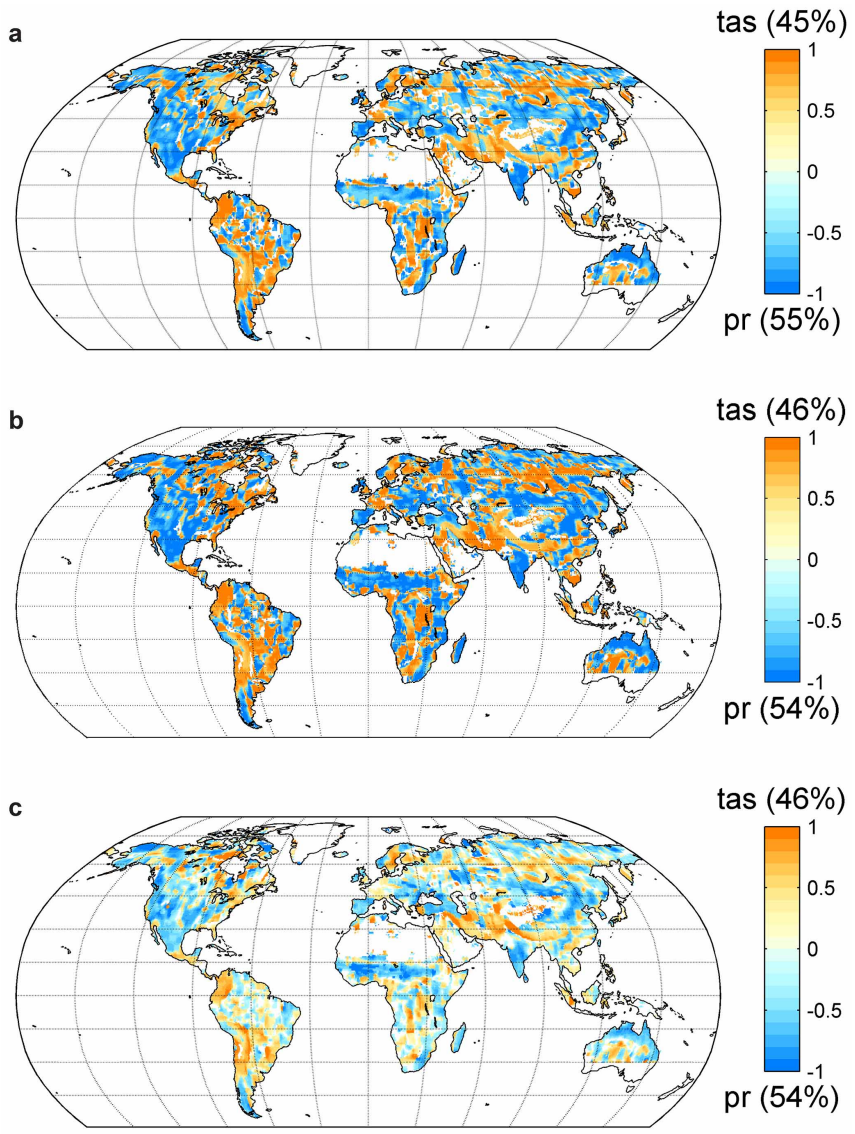

Extended Data Figure 4 | Maximum relative importance of temperature and precipitation in the explained variance of turnover times of carbon. **a**, Maximum relative importance of temperature (tas) or precipitation (pr) in the explained variance of τ using the LMG method. **b**, Relative importance of temperature (tas) or precipitation (pr) in improving the residual sum of squares of local bivariate regressions of τ against tas and pr. **c**, Normalized slopes of the bivariate regression between τ and precipitation and temperature, using a stepwise regression approach. Also, here the slopes correlate significantly with the strength of the association between the two variables. The fraction of land grid cells with stronger significant correlations to temperature and precipitation are indicated above (for tas) and below (for pr) the colour bar.

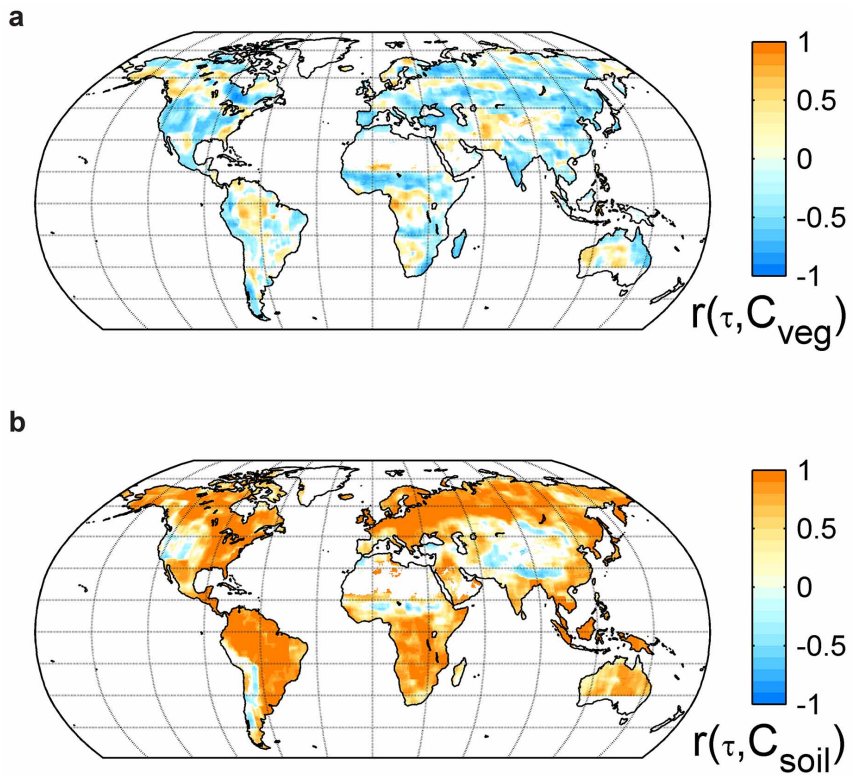

Extended Data Figure 5 | Moving-window correlation between turnover times of carbon in terrestrial ecosystems and vegetation, and soil carbon stocks. Moving-window correlation between τ and vegetation stocks (**a**); and between τ and carbon in soils (**b**). In general, τ correlates negatively with vegetation (**a**), indicating shorter turnover times with a higher proportion of carbon in the vegetation. The majority of the patterns are consistent with the overall reduction of residence times in ecosystem carbon given allocation to vegetation pools (shorter lived by comparison with soil carbon pools). Conversely, the significance of soil carbon stocks in explaining the spatial variability of τ is pervasive (**b**). These results translate the trends in increasing τ with allocation of assimilated carbon to more persistent carbon pools.

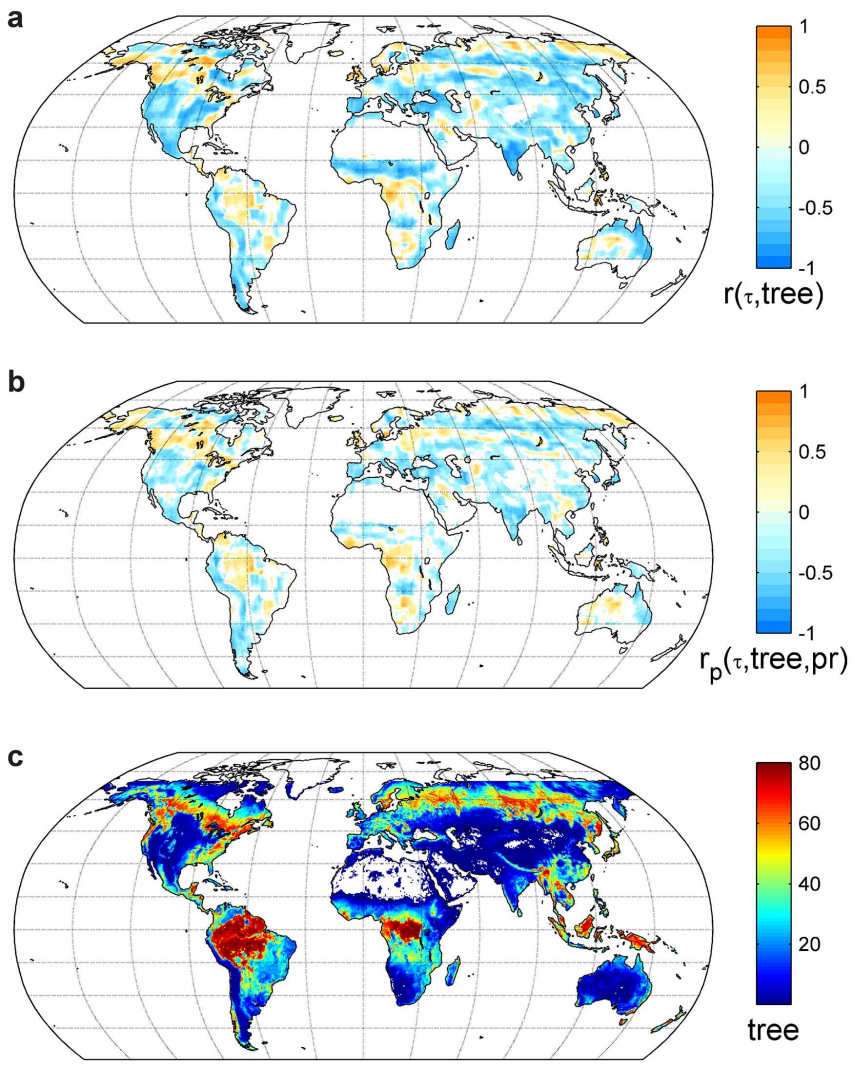

Extended Data Figure 6 | Pearson correlations between turnover times of carbon in terrestrial ecosystems and tree cover, also controlled for the variability in precipitation. **a**, Pearson correlations between τ and tree cover. The prevalence of strong negative correlations suggests that the association could be mediated by precipitation variability. **b**, Controlling for precipitation still showed many of those negative correlation regions. These negative correlations are most clear in regions where tree cover is not so high or where spatial variability seems higher. **c**, Map of tree cover percentage from MODIS[71].

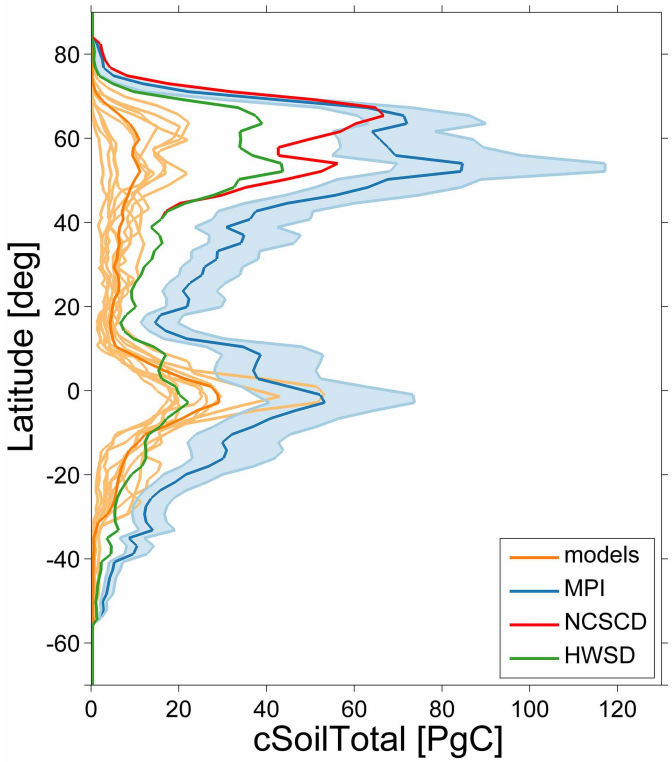

Extended Data Figure 7 | Latitudinal profiles of total soil organic carbon as simulated by CMIP5 models and from the observation-derived data ensembles. Latitudinal profiles of total soil organic carbon as simulated by CMIP5 models and from data: HWSD[33] (1 m depth), NCSCD[38,39] (1 m depth) and this study (MPI, to full soil depth).

Extended Data Table 1 | Estimates of total ecosystem carbon for the globe and discriminated per biome

	Total stocks (PgC)			Carbon density (kgC m^{-2})		
Biome type	**Mean**	**P 2.5**	**P 97.5**	**Mean**	**P 2.5**	**P 97.5**
Tropical forests	702	573	899	35.0	28.6	44.8
Temperate forests	292	235	382	23.4	18.8	30.6
Boreal forests	505	431	696	34.2	29.2	47.1
Tropical savannahs and grasslands	338	257	467	17.7	13.4	24.4
Temperate grasslands and shrublands	182	145	239	16.7	13.3	22.0
Deserts	250	189	346	9.4	7.1	13.0
Tundra	156	106	186	20.5	14.0	24.5
Croplands	362	279	494	23.9	18.4	32.6
Wetlands	20	15	27	21.1	16.3	28.6
Total	**2807**	**2252**	**3662**	**22.0**	**17.7**	**28.7**

Estimates of total ecosystem carbon per biome. Biomes defined according to Prentice *et al.*[66] as in Beer *et al.*[67]. The ranges report the 2.5th (P 2.5) and 97.5th (P 97.5) percentiles from each ensemble member aggregated by biome.

Extended Data Table 2 | Estimates of total ecosystem carbon turnover times, stocks and fluxes of carbon for each of the CMIP5 models and correlations with data

	Global estimates								Correlation (r^2)							
Model	τ	C_{total}	C_{soil}	C_{veg}	**GPP**	**NPP**	τ_{veg}	τ_{soil}	τ	C_{total}	C_{soil}	C_{veg}	**GPP**	**NPP**	τ_{veg}	τ_{soil}
bcc-csm1-1	12.1	1507	1037	462	124	64	3.8	16.3	0.42	0.23	0.12	0.66	0.74	0.65	0.17	0.55
CanESM2	16.0	2075	1542	527	130	64	4.1	24.1	0.28	0.12	0.05	0.46	0.37	0.51	0.13	0.27
CCSM4	8.5	1101	573	522	129	45	4.1	12.6	0.17	0.22	0.03	0.65	0.75	0.77	0.14	0.42
GFDL-ESM2G	12.4	2075	1419	651	168	104	3.9	13.7	0.34	0.05	0.04	0.40	0.60	0.50	0.01	0.42
HadGEM2-ES	11.3	1567	1068	496	139	73	3.6	14.6	0.30	0.22	0.07	0.68	0.76	0.64	0.18	0.15
inmcm4	16.6	2277	1676	594	137	67	4.4	24.9	0.12	0.16	0.08	0.53	0.81	0.79	0.04	0.46
IPSL-CM5A-MR	12.3	2029	1395	629	165	82	3.8	16.9	0.26	0.28	0.15	0.42	0.68	0.38	0.13	0.52
MIROC-ESM	22.7	2923	2560	358	129	61	2.8	42.0	0.28	0.15	0.16	0.50	0.67	0.54	0.11	0.54
MPI-ESM-LR	19.7	3374	3036	336	170	88	2.0	33.9	0.46	0.001	0.003*	0.60	0.65	0.66	0.13	0.21
NorESM1-M	8.9	1153	608	538	129	46	4.2	13.1	0.18	0.31	0.13	0.61	0.71	0.72	0.13	0.47
Data (P10)	18.8	2394	1952	437	126.0	43	3.5	33.8								
Data (mean)	22.1	2797	2352	445	126.7	54	3.5	45.8								
Data (P90)	26.9	3401	2958	452	127.2	64	3.6	59.4								
Models (P10)	8.7	1131	591	346	122.9	46	2.4	12.9								
Models (mean)	14.0	1975	1466	509	140.3	69	3.7	21.3	0.38	0.45	0.26	0.79	0.85	0.82	0.18	0.59
Models (P90)	21.3	3113	2767	639	169.2	96	4.3	38.1								
Mean difference [%]	-36	-29	-38	14	11	27	4	-54								

Estimates of total ecosystem carbon turnover times (τ), carbon stocks (C_{total}, PgC), soil stocks (C_{soil}, PgC), vegetation stocks (C_{veg}, PgC), gross primary productivity (GPP, PgC yr^{-1}), net primary productivity (NPP, PgC yr^{-1}), τ_{veg} (C_{veg}/GPP, yr) and τ_{soil} (C_{soil}/NPP, yr) for each of the CMIP5 models, and correlations with data at each native model resolution (squared correlations weighted by area with removal of 2% of outliers). Global ensemble estimates (at the common ensemble spatial grid) for data and models, including lower (10th percentile, P 10) and upper (90th percentile, P 90) envelopes. For correlation estimates, we removed deserts (according to ref. 68) and low GPP values (below 10 gC m^{-2} yr^{-1}). Low productivity values were also removed for the global estimates of τ, τ_{soil} and τ_{veg}.
* Non-significant correlations, $P > 0.05$.